Research Article Vol. 33, No. 7 / 7 Apr 2025 / Optics Express 16305
Optics EXPRESS

Dynamic spectral tailoring of a 10 GHz laser frequency comb for enhanced calibration of astronomical spectrographs

POOJA SEKHAR,[1,2,5] CONNOR FREDRICK,[1,2,3] PETER ZHONG,[1] ABIJITH S. KOWLIGY,[4] ARMAN CINGÖZ,[4] AND SCOTT A. DIDDAMS[1,2,6]

[1]Electrical, Computer and Energy Engineering, University of Colorado Boulder, Colorado 80309, USA
[2]Department of Physics, University of Colorado Boulder, Colorado 80309, USA
[3]National Institute of Standards and Technology, Boulder, Colorado 80305, USA
[4]Vector Atomic, Inc. 6870 Koll Center Pkwy, Pleasanton, California 94566, USA
[5]pooja.sekhar@colorado.edu
[6]scott.diddams@colorado.edu

Abstract: Laser frequency combs (LFCs) are an important component of Doppler radial velocity (RV) spectroscopy that pushes fractional precision to the 10^{-10} level, as required to identify and characterize Earth-like exoplanets. However, large intensity variations across the LFC spectrum that arise in the nonlinear broadening limit the range of comb modes that can be used for optimal wavelength calibration with sufficient signal-to-noise ratio. Furthermore, temporal spectral-intensity fluctuations of the LFC, that are coupled to flux-dependent detector defects, alter the instrumental point spread function (PSF) and result in spurious RV shifts. To address these issues and improve calibration precision, spectral flattening is crucial for LFCs to maintain a constant photon flux per comb mode. In this work, we demonstrate a dynamic spectral shaping setup using a spatial light modulator (SLM) over the wavelength range of 800–1300 nm. The custom shaping compensates for amplitude fluctuations in real time and can also correct for wavelength-dependent spectrograph transmission, achieving a spectral profile that delivers the constant readout necessary for maximizing precision. Importantly, we characterize the out-of-loop properties of the spectral flattener to verify a twofold improvement in spectral stability. This technique, combined with our approach of pumping the waveguide spectral broadener out-of-band at 1550 nm, reduces the required dynamic range. While this spectral region is tailored for the LFC employed at the Habitable-zone Planet Finder (HPF) spectrograph, the method is broadly applicable to any LFC used for astronomical spectrograph calibration.

1. Introduction

The search for Earth-analogs using the radial velocity technique requires precision at the cm/s level, corresponding to fractional Doppler shifts of 10^{-10}. This precision amounts to a shift in the centroid of stellar absorption lines at the level of 10's of kHz. Functionally, this requires measuring a spatial shift of the dispersed spectrum by about 10^{-5} of a pixel in the detector array at the spectrograph image plane. One of the critical requirements for achieving this demanding precision is the long-term frequency stability of the calibration source, ideally over many years of nightly operation.

In this regard, laser frequency combs (LFCs) have emerged as ideal calibration sources for astronomical spectrographs since the frequency of all comb teeth can be referenced to a GPS-disciplined atomic clock [1–4]. Two critical requirements for "astrocombs," which are LFCs designed specifically for astronomical spectrographs, include tens of gigahertz (GHz) mode spacing and spectral coverage exceeding 500 nm. The latter requirement of broadband spectral

#557365 https://doi.org/10.1364/OE.557365
Journal © 2025 Received 6 Feb 2025; revised 15 Mar 2025; accepted 20 Mar 2025; published 3 Apr 2025

Optics EXPRESS

coverage is realized using dispersion-engineered nonlinear media like photonic crystal fibers [5], highly nonlinear single-mode fibers [6,7] or waveguides [8]. However, the intensity profile of the resulting broadband supercontinuum is not flat and often exhibits wavelength-dependent variations over several orders of magnitude. Additionally, the spectral envelope can fluctuate over time due to changes in the peak power of the pump and the aging of components, particularly the amplifiers and nonlinear media.

These intensity fluctuations in the comb modes change the continuum level in the detector readout asymmetrically due to overlapping contributions from adjacent lines. This, combined with flux-dependent detector defects such as nonlinear response, brighter-fatter effect, persistence contamination from the previous exposure, and intra- and inter pixel quantum efficiency variations, result in changes to the shape of the instrumental point spread function (PSF) [9–11]. All of these variations can lead to wavelength calibration errors and spurious RV shifts. Additionally, it is essential to maintain a uniform flux distribution while scanning the laser frequency comb (LFC) across the spectrograph, as demonstrated in our previous work [12]. Such scanning is crucial for characterizing the impact of intrapixel quantum efficiency variations on the PSF profile, which is key to improving RV precision and accuracy. Large intensity variations exceeding 20 dB across the spectrum also lead to detector saturation at certain wavelengths, while other comb modes with lower intensity may be buried in noise. If spectral shaping techniques are unavailable, the flux level of the comb needs to be uniformly attenuated by a factor, so as to keep the most intense comb mode below saturation. This will reduce the number of photoelectrons collected across the entire spectrum and as a result, increase the photon noise floor.

To address the above issues, a dynamic spectral flattener is required for astrocombs. This flattener ensures a uniform photon flux across all comb modes, thereby maximizing the achievable signal-to-noise ratio (SNR) and enhancing the calibration precision of astronomical spectrographs. Moreover, a stable and uniform photon flux of LFC also enables the systematic subtraction of scattered LFC contributions on the stellar spectrum.

Control of comb mode intensities has been achieved using programmable attenuators such as liquid-crystal based spatial light modulators (SLM) [13–15]. Apart from astronomy, similar spectral control systems using SLMs are employed in temporal pulse shaping [16], optical communications as a wavelength selective switch [17] and in the pulse compression of frequency combs via higher-order dispersion compensation [18]. SLMs are also extensively used in a variety of other applications, such as confocal microscopy for imaging biological systems [19], arbitrary waveform generation [20], programmable bandpass filtering [21], 2D spectroscopy [22], white light beam shaping [23] and steering for material processing [24], as well as in holography [25] and optical tweezers [26], to cite a few. Compared to these methods, our spectral shaping technique offers both larger bandwidth and higher degree of intensity stability over extended periods. Recently, this technique of spectral flattening of laser frequency combs has also been integrated as an arrayed waveguide grating (AWG) on silicon nitride (SiN) and thin-film lithium niobate platform over narrower bandwidths around 1550 nm [27,28].

Our immediate focus for this work relates to the 30 GHz electro-optic comb spanning 800 - 1300 nm that is used as the calibration source for the Habitable Zone Planet Finder spectrograph [8,29,30]. The LFC at the HPF has been running reliably for the past six years, with an uptime exceeding 98%, unparalleled by other astrocomb systems. However, the comb mode intensities are controlled with a static spectral mask and can vary by as much as a factor of two with time. Additionally, the readout from the detector, common to all spectrographs, exhibits a characteristic echelle blazing pattern that depends on the optics and grating employed, as shown in Fig. 1(a).

To address these shortcomings, here we implement custom spectral tailoring using an SLM that compensates for the echelle pattern, ensuring a constant flux level across the comb modes on readout from the detector, as illustrated in Fig. 1(b). Furthermore, we have demonstrated an improvement in fractional intensity stability of our laboratory comb system by approximately a

Optics EXPRESS

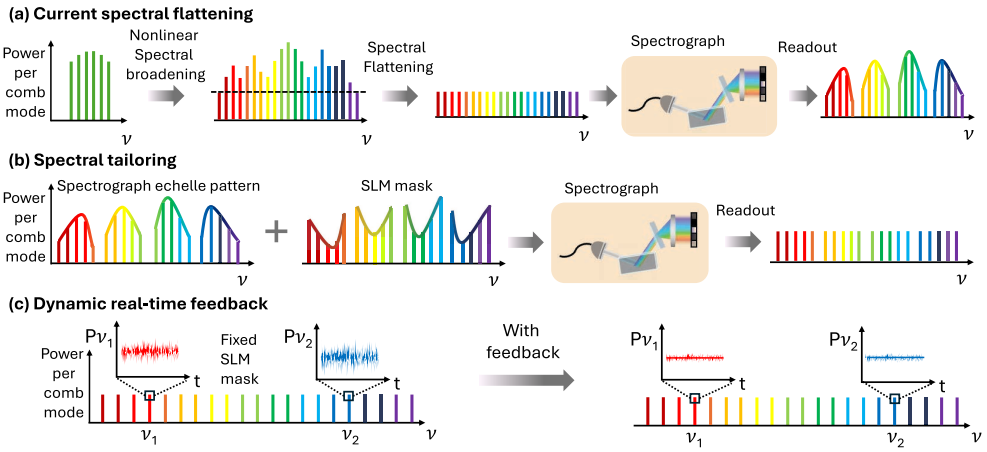

Fig. 1. Custom spectral tailoring and dynamic real-time feedback on an astrocomb. (a) Schematic illustrating the generation and spectral flattening of current state-of-the-art "deployed" astrocombs. A narrowband high-repetition rate comb is generated from a filtered mode-locked laser, electro-optic modulator (EOM), or microresonator. This comb is spectrally broadened using highly-nonlinear fibers or nanophotonic waveguides, resulting in supercontinuum with inherent intensity variations, often exceeding factors of 20-30 dB across the wavelength band. A spectral flattener is implemented to equalize the flux of all comb modes across the entire spectral range of the detector. However, the detector's readout features a characteristic blazing pattern across different echelle orders and exhibits wavelength-dependent responsivity. (b) Schematic demonstrating custom spectral tailoring using a spatial light modulator (SLM). The SLM mask is tailored to compensate for the echelle pattern and the wavelength-dependent responsivity of the spectrograph, achieving a uniform flux across the detector on readout. (c) Illustration of the exaggerated effect of dynamic real-time flattening on the intensity variation of comb modes, highlighting the improvement in photon flux consistency.

factor of two through a dynamic real-time feedback loop to the SLM (Fig. 1(c)). Importantly, the impact of spectral flattening feedback has been evaluated through an out-of-loop measurement with an optical spectrum analyzer (OSA). Finally, we demonstrate these advances in spectral control across 800-1300 nm with an electro-optic comb pumped at 1.55 μm, instead of the "in band" pumping at 1.064 μm that currently exists at the HPF. This presents a significant advantage by reducing the required dynamic range for the spectral flattening to less than 12 dB, in contrast to over 20 dB with 1.064 μm pumping. In the future, we plan to employ these advantages to upgrade the performance of the calibration system at HPF.

2. Spectral flattening setup

For this study, the LFC source is a 10 GHz resonant electro-optic comb pumped at 1550 nm. The comb is amplified to 5 W and temporally compressed to a duration of 50 fs. Further details on the comb system can be found in [31]. The compressed 10 GHz pulses are then launched into a hybrid SiN waveguide to generate a supercontinuum spanning 780 - 1700 nm as shown in Fig. 3(d). In the current setup using out-of-band pumping at 1550 nm, achieving the peak powers necessary to generate a supercontinuum spanning 800–1300 nm at 30 GHz repetition rates as in HPF is not easily accomplished. As a result, we have employed LFC at a reduced repetition rate of 10 GHz. The SiN waveguide is 23.5 mm long with a thickness of 800 nm. It features a hybrid design consisting of an initial 15 mm long segment with a width of 2.6 μm

Optics EXPRESS

followed by a section that is 8.5 mm long and 4.8 μm wide. This hybrid dispersion profile along the waveguide's propagation length facilitates the generation of a broadband and relatively flat spectrum [32,33]. Additionally, pumping at 1550 nm significantly reduces the dynamic range required for spectral flattening to less than 12 dB across the entire HPF spectral bandwidth of 800 - 1300 nm, as the pump peak at 1550 nm lies outside the desired wavelength range. This is in contrast to previous systems that had their pump within the desired wavelength range and required a larger dynamic range for spectral flattening [8,13,14].

Figure 2 is a schematic of our experimental setup. This approach to Fourier-domain optical pulse shaping is similar to previous works, such as [8,13,14,34]. The broadband frequency comb is collimated and polarized at 45° with respect to the liquid crystal axis of the SLM using a half-wave plate and a linear polarizer. The beam is then dispersed by a transmissive volume holographic grating and the individual spectral components are focused onto the SLM using a cylindrical lens of 5 cm focal length (f). The reflective spatial light modulator (SLM) used in this study is a Meadowlark model: E19x12-600-1300-OH, with 1920 × 1200 pixels covering an active area of 15.36 × 9.60 mm. The reflected light from the SLM is re-collimated and recombined by the cylindrical lens and grating respectively. Both the grating and SLM are positioned at a distance f from the cylindrical lens, forming a 4f configuration [16]. The original grating employed for all the measurements presented in this paper except the one in Fig. 5 has 600 lines per mm and diffraction efficiency over a narrow bandwidth. To address this, it was replaced with a grating, with 500 lines per mm, that operates across the full 800–1300 nm bandwidth. Additional information on the two gratings used can be found in section 4.

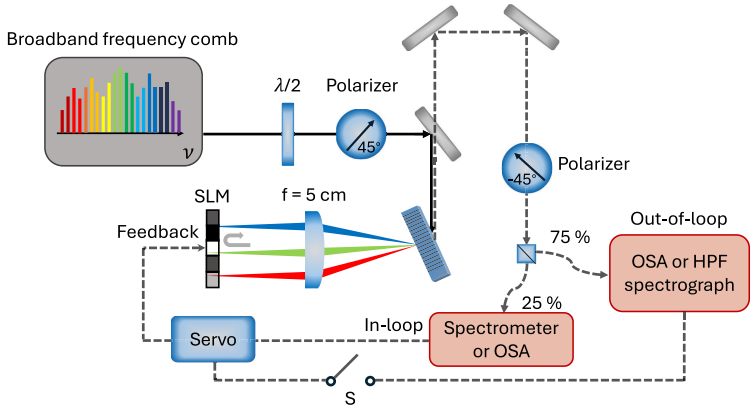

Fig. 2. Experimental setup for spectral flattening. $\lambda/2$: half-wave plate; SLM: spatial light modulator; OSA: optical spectrum analyzer; HPF: Habitable-zone planet finder spectrograph; S: switch. The switch is used to update the target spectrum for feedback based on the spectrograph or OSA readout.

The broadband frequency comb is spread across the longer edge of the SLM achieving a spectral resolution of 0.4 - 0.6 nm across the wavelength range of 800 - 1300 nm. The resolution achieved with this setup at 1064 nm is ~ 130 GHz, which is greater than the comb mode spacing. For additional details on the spectral flattening setup, refer to Figure S1 in Supplement 1.

The voltage applied to each pixel of the SLM induces a rotation of the liquid crystals. This adds a phase shift along one polarization axis, thereby allowing the SLM to function as a variable waveplate. A cross-polarizer at the output converts the polarization rotation induced by the SLM into a wavelength-dependent attenuation. The output light is then split using a fiber-integrated 75:25 multimode splitter with a core diameter of 50 μm. The 1m long fiber splitter transmits >99% of the input light across 650 - 2000 nm. The 25% port is sent to a

Optics EXPRESS

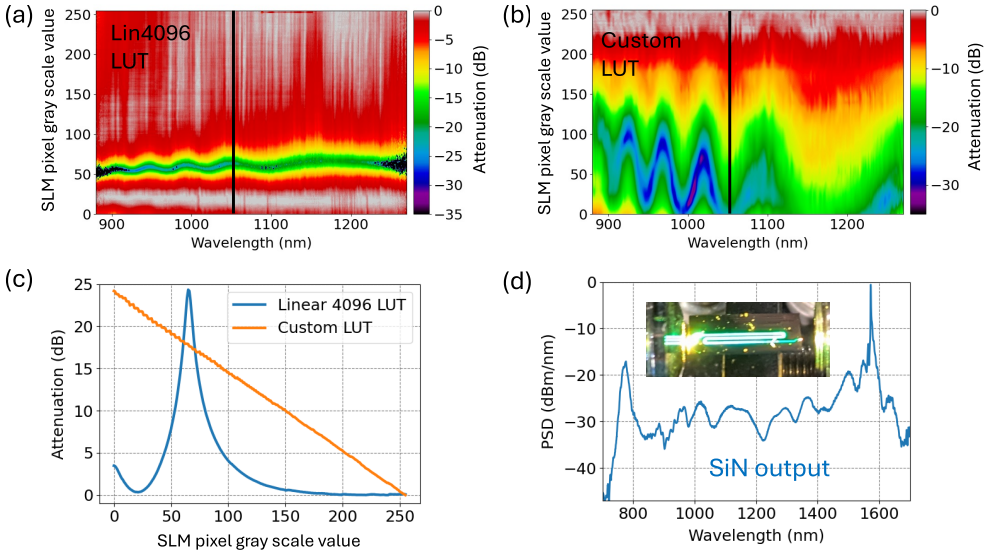

Fig. 3. Attenuation calibration of the spatial light modulator (SLM). The achieved attenuation range across the supercontinuum spanning 870 - 1280 nm on varying the grayscale value uniformly across all pixels of the SLM using, (a) linear look-up-table (LUT) varying from 0 to 4096 in increments of 16, and (b) Custom LUT designed for log-linear variation in attenuation from its minimum to maximum value across all wavelengths. (c) Attenuation at a central wavelength of 1064 nm using the above two LUTs. (d) Uncorrected supercontinuum output directly from the silicon nitride (SiN) waveguide pumped by a 10 GHz electro-optic comb at 1550 nm. Photo shows the top-view of the SiN chip generating the supercontinuum.

grating-based spectrometer with an InGaAs linear array to monitor the output spectrum and provide feedback to the SLM for real-time intensity adjustments. The remaining 75% port is used to measure the flattened LFC in an "out-of-loop" optical spectrum analyzer (OSA). When used at the telescope site, the OSA would be replaced by the astronomical spectrograph.

3. Calibration of SLM

The spectral flattening technique using an SLM involves two major calibration steps: (i) Attenuation calibration, which maps the power transmitted at a particular wavelength as a function of the voltage applied to the SLM pixels, and (ii) Wavelength calibration, which maps the pixel column number to a specific wavelength. The section below describes both calibration procedures in detail.

3.1. Mapping attenuation to grayscale value on SLM

In order to setup the spectral flattening system and perform the attenuation calibration for maximum dynamic range, we start with a continuous wave (CW) laser at the center wavelength of 1064 nm. The first polarizer is aligned at 45° with respect to the liquid crystals, while the second polarizer is cross-polarized to minimize the power transmitted through the combined polarizer system. The spectrometer port of the 25/75 beamsplitter shown in Fig. 2 is replaced by a powermeter to measure the transmitted power.

The SLM has a 12-bit controller. There are 4096 possible voltage levels that can be applied to the liquid crystals to achieve varying degrees of phase shift. However, the computer-display interface of the device is limited to 8-bits per pixel, so a look up table (LUT) is used to map the 256 grayscale values to discrete voltage levels. Only 256 of the 4096 values are accessible

Optics EXPRESS

through any one LUT. The main purpose of the attenuation calibration is to choose a LUT that gives the greatest dynamic range and resolution. In this system, the LUT referred to as 'Lin4096' ranges from 0 to 4096 in steps of 16. Recalibration of the LUT is necessary to achieve the desired phase shift for most applications.

To optimize the polarization of input light to the SLM for maximum dynamic range of attenuation, we follow the procedure outlined below. First, we set the grayscale value uniformly across the SLM pixels to the value that results in the lowest transmitted power. Next, we fine-tune both the output and input polarizers to further minimize the transmitted power measured. The half-wave plate is then adjusted to align the input light polarization with the axis of the first polarizer. Following these adjustments, we gradually change the grayscale value across the SLM pixels from 0 to 255, measuring the transmitted power at each step and recording the dynamic range achieved. These steps of tuning the SLM grayscale scale, adjusting the polarizers, and fine-tuning the half-wave plate are repeated until the maximum dynamic range is obtained.

With the optical components of the system fixed, the CW laser and powermeter are replaced by the broadband LFC and OSA respectively. The grayscale value is varied from 0 to 255 using the Lin4096 LUT and the resulting power variation of the supercontinuum across 870 - 1280 nm is recorded on the OSA. The maximum intensity at each wavelength is noted and the relative attenuation across the entire wavelength range is presented in Fig. 3(a). The results indicate that the net phase shift wraps through 2π, demonstrating that the Lin4096 LUT does not provide a linear attenuation with respect to the pixel value. This LUT covers a phase shift larger than required and does not allow small step sizes as needed to make fine adjustments in intensity.

Consequently, we generate a custom LUT such that the grayscale values 0-255 correspond to the minimum and maximum transmitted power at the center wavelength of 1064 nm. The attenuation map generated using this custom LUT is displayed as a false color image in Fig. 3(b). The attenuation achieved at 1064 nm using both the LUTs is also plotted in Fig. 3(c). The system achieves a maximum attenuation of 25 dB at 1064 nm and even reaches 30 dB at 1 μm, with step sizes as low as 0.09 - 0.1 dB. Since liquid crystals are not achromatic, the induced phase shift is wavelength-dependent as shown in Fig. 3(b). As a result, we record the grayscale values corresponding to the minimum and maximum transmitted power at each wavelength and use that information to bound the range of the spectral flattening algorithm accordingly.

3.2. Mapping wavelength to SLM pixel column number

Wavelength calibration is performed to identify the center wavelength corresponding to each column pixel number of the SLM, which is perpendicular to the axis along which input light is dispersed. Initially, all the pixels are uniformly set to 255, corresponding to nearly maximum transmitted power across all wavelengths and the measured spectrum is recorded. Then a set of 20 pixel columns are sequentially set to zero to achieve maximum attenuation. In this way, the entire SLM is mapped in steps of 20, with the transmission spectra recorded at each step as shown in Fig. 4(a).

The difference between the transmitted spectra at each step and the spectrum with no attenuation is calculated and fitted with a Gaussian function. The center wavelength is then attributed to the mean of the column pixels set to maximum attenuation, represented by the blue dots in Fig. 4(b). The measured wavelength-to-pixel data is fitted with an extrapolated smooth spline (red trace in Fig. 4(b)), which is used as the wavelength calibration curve for the spectral flattening algorithm. The residuals to the fit is within 0.5 nm, which is less than the full-width at half-maximum (FWHM) of the optical resolution of the spectral flattening setup as shown in Supplement 1, Fig. S3.

This precise calibration is necessary to prevent intensity adjustments at a neighboring wavelength instead of the desired one, which can result in undesirable modulations on the LFC

Optics EXPRESS

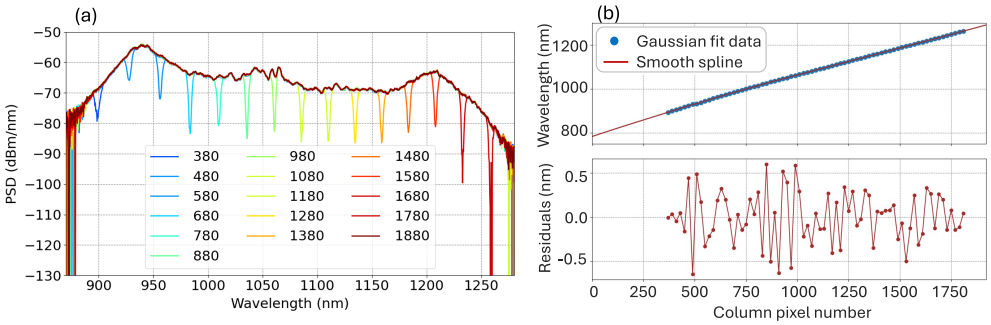

Fig. 4. Wavelength-to-pixel calibration of SLM. (a) The SLM is configured for maximum attenuation column-wise in steps of 20. Legends indicate the column numbers. The resulting transmission spectra from the spectral flattener recorded by the optical spectrum analyzer (OSA) at each step are overlaid. (b) The blue dots in the top plot show the center wavelengths obtained by fitting a Gaussian to the corresponding transmission spectra from (a). The red line in the top plot indicates a smooth spline fit to the center wavelengths, while the bottom plot displays the residuals between the smooth spline and the Gaussian fit centers.

envelope during prolonged operation of the spectral flattening algorithm [13]. This wavelength calibration procedure has been performed separately using both the OSA and spectrometer.

4. Demonstration of real-time spectral shape tailoring

The goal of the spectral flattening setup is to maintain a constant photon flux for all comb modes across the spectrograph bandwidth, which is 800 - 1300 nm for the HPF. The spectral flattening output is measured on an OSA or spectrometer in terms of spectral density (in mW per nm or counts per nm respectively). The number of comb modes per nanometer is inversely proportional to the square of the wavelength, and the photon energy is proportional to the inverse of wavelength. Thus, a constant power spectral density corresponds to the photon flux around a comb mode being directly proportional to the third power of the wavelength. This is the photon flux (number of photons/sec) per comb mode available for the astronomical spectrograph.

To compensate this, the reference set in the SLM has a negative slope with respect to wavelength as illustrated by the black dashed line in Fig. 5(a). To achieve spectral shaping over the entire 800–1300 nm range as shown in Fig. 5, the original grating, which had efficiency over a narrow bandwidth, was replaced. A comparison of the insertion loss (IL) for the spectral flattening setup, using both gratings, is presented in the bottom plot of Fig. 5(b). The measured insertion loss is without including any additional attenuation from the SLM.

4.1. Spectral flattening feedback loop

Using the wavelength-dependent attenuation-to-pixel value calibration and wavelength-to-pixel number map, a spectral flattening feedback algorithm was developed in Python. The process begins by recording the spectrum on the in-loop spectrometer without any spectral shaping. The blue trace in Fig. 5(a) shows the spectrum measured on an out-of-loop OSA before flattening. The algorithm calculates the difference between the measured spectrum and the target (reference) spectrum across the supercontinuum spanning 800 - 1300 nm. Employing the two calibration curves of Fig. 3(b) and Fig. 4(b), the algorithm applies the pixel value corresponding to the required attenuation at each specific wavelength to the particular pixel column in the SLM. It is crucial to restrict the range of grayscale pixel values at each wavelength to its minimum and maximum attenuation range to ensure the feedback maintains the correct sign.

Optics EXPRESS

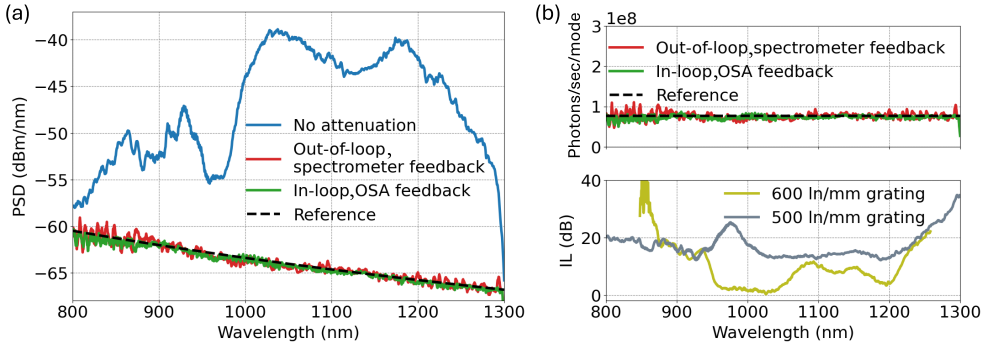

Fig. 5. Measured spectrum of a 10 GHz laser frequency comb (LFC) spectrum on the OSA after spectral flattening through both in-loop and out-of-loop cases. (a) Power spectral density (PSD in dBm/nm) of the output LFC from the spectral flattener, comparing results with and without applying attenuation. (b) Constant photon flux per comb mode (photons/sec/mode in linear scale) of the spectral flattener outputs from (a). The out-of-loop measurement (red curve) reflects the LFC output recorded on the OSA, while feedback to the spatial light modulator (SLM) is obtained from the spectrometer. In contrast, for the in-loop measurement (green curve) both the output and feedback to the spectral flattener are provided by the same instrument, the OSA. The bottom plot compares the insertion loss (IL) of the spectral flattening setup using the two gratings.

A single iteration achieves an intensity level within 3 dB of the target. This procedure is repeated in a feedback loop, with a new spectrum recorded after each iteration. The updated wavelength-dependent attenuation is recalculated, and the corrected grayscale pixel values are applied to the corresponding column pixels. The spectrum measured on the OSA reaches a steady state in less than 10 iterations.

4.2. In-loop vs out-of-loop measurements

The resulting flattened spectrum represented by the green and red traces in Fig. 5(a) are obtained when feedback is applied from the OSA and the spectrometer respectively. We refer to these two cases as in-loop or out-of-loop measurements, depending on whether the feedback and flattened spectrum are measured using the same instrument or two different instruments. This distinction is important to make and test. In actual use with an astronomical spectrograph (such as the HPF), the calibration spectrum from the HPF will be out-of-loop and acquired on a much longer timescale than the in-loop spectrometer-based feedback.

In the case of an out-of-loop measurement, a precise intensity cross-calibration measurement needs to be performed between the two instruments to establish a new target spectrum in the SLM [14,35]. A single iteration takes approximately 1.6 seconds when feedback is applied from the OSA, while it is an order of magnitude faster (around 0.3 seconds) using the spectrometer for feedback. The degree of flatness achieved is within 1.6 dB for the in-loop measurement and 2.6 dB for the out-of-loop measurement across the wavelength range of 860 - 1300 nm. Figure 5(b) presents these measurements on a linear scale, displaying the flattened photon flux per comb mode. This clearly illustrates that the degree of flatness for the out-of-loop measurement is not as small as that for the in-loop measurement, with more high-frequency intensity fluctuations observed. These fluctuations are related to the accuracy of the intensity cross-calibration between the OSA and the spectrometer, which includes wavelength-dependent differences in responsivity of the two. The accuracy is further limited by the lower sensitivity of the spectrometer compared to the OSA and the accuracy of wavelength calibration. For additional details, refer to Figure S2 in the Supplement.

Optics EXPRESS

4.3. Impact of real-time feedback on spectral stability

The 10 GHz LFC in this laboratory setup is not frequency stabilized to the GPS and the power levels at each step of broadening are not monitored in contrast to the system installed with the HPF at the Hobby-Eberly telescope [8]. The only feedback control in the experimental setup, aside from the SLM, is to the NanoMax^{TM} stage, which is actively piezo-controlled to maintain the same coupling efficiency to the SiN waveguide with the high average powers during measurements (typically 3 W). We observe that fractional intensity fluctuations at certain wavelengths of the supercontinuum can reach as high as 20%. Figure 6 compares the stability of power spectral density of the supercontinuum across 910 - 1260 nm with (a) and without (b) real-time feedback from the OSA through an in-loop measurement. The traces in the top plots are recorded every 10 seconds over a duration of one hour, while a single feedback iteration takes approximately 1.6 seconds.

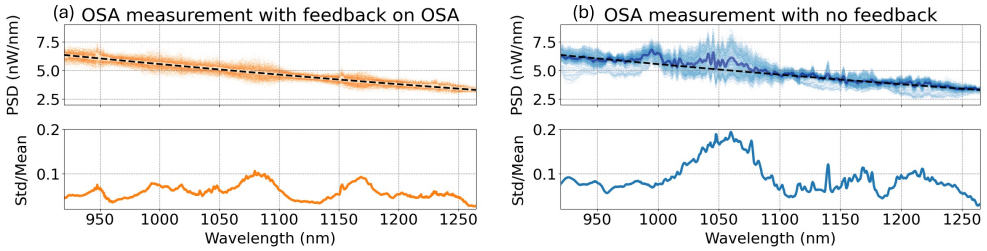

Fig. 6. Comparison of the flattened 10 GHz laser frequency comb (LFC) spectrum on an optical spectrum analyzer (OSA) after the spectral flattener through an in-loop measurement: (a) with, and (b) without real-time feedback. The top plots illustrate the variation in power spectral density of the comb over a one-hour measurement period, while the bottom plots show the corresponding standard deviation by mean values. Notably, the implementation of real-time feedback reduces the fractional intensity fluctuations by almost a factor of two.

The results indicate that real-time feedback reduces fractional intensity fluctuations by a factor of two. The mean value of fractional intensity fluctuations is 5% in the presence of real-time feedback, which may be limited by the technical noise of the measurement system, not stabilized within the feedback iteration time. This may not pose a problem for actual observations at the HPF or another telescope site, where stellar and calibration spectra are typically acquired with an integration time of 5-10 minutes. The Allan deviation of intensity fluctuations at an averaging time of 10 minutes is nearly an order of magnitude lower than at 10 seconds in the presence of real-time feedback as shown in Supplement 1. The stability of feedback loop and the degree of spectral flatness were also monitored for over 6 hours, showing no signs of degradation.

4.4. Compensation of the echelle blazing pattern of an astronomical spectrograph response

Every astronomical spectrograph exhibits a characteristic blazing pattern that depends on the grating and optics used. Each echelle order has a specific bandwidth, with gaps in the spectral readout between different orders. The top plot in Fig. 7(a) shows a fit to the typical echelle response from the HPF spectrograph. As a result, even a flattened LFC spectrum shown in Fig. 5(b) does not translate to a constant flux per comb mode in the spectrograph readout. In this work, we utilize the spectral flattener described above in Fig. 1 to tailor the LFC spectrum in real-time, compensating for this echelle response to achieve a constant LFC flux per comb mode in the spectrograph readout.

The in-loop (red trace) and out-of-loop (blue trace) measurements of this inverse echelle response (dashed black trace) are plotted in Fig. 7(b). The results demonstrate a good degree

Optics EXPRESS

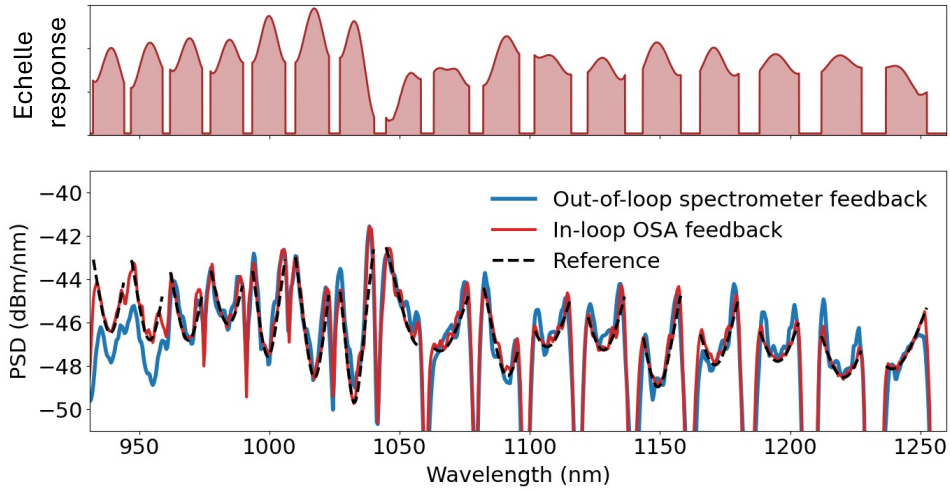

Fig. 7. Compensation of spectrograph response. The top plot represents a fitted model of the echelle response data from the HPF spectrograph. The bottom plot shows the measured output of the laser frequency comb (LFC) from the spectral flattener on an optical spectrum analyzer (OSA) after applying a spatial light modulator (SLM) mask to compensate for the blazing pattern of different echelle orders in the HPF spectrograph. The blue and red traces on the bottom plot represent the feedback to the SLM obtained from a spectrometer and OSA respectively.

of agreement with the target curve. The disagreement between the out-of-loop measurement and the target may be attributed to the intensity cross-calibration and the lower sensitivity of the spectrometer as compared to OSA (see Fig. S2 in Supplement 1). For spectrographs like HPF with gaps in echelle orders, this approach of spectral shaping may also reduce the impact of scattered light contributions on the stellar spectrum from the comb lines outside the echelle orders.

5. Conclusion

In summary, we have demonstrated a dynamic spectral flattening setup for astrocombs, using a spatial light modulator, as a critical aspect of radial velocity spectroscopy aimed at achieveing cm/s RV precision. In contrast to the current LFC setup at HPF that spans 800 - 1300 nm, this work provides two key advancements. First, custom spectral tailoring is used to compensate for the characteristic echelle pattern of the spectrograph. This tailoring helps maintain a constant flux readout of the LFC from the detector, while also reducing the contamination of scattered comb light on the stellar spectrum by attenuating the comb light between the echelle orders. Second, real-time feedback to the SLM mitigates spectral intensity variations over time, improving the spectral stability by nearly a factor of two.

An additional important aspect of our work is the analysis of the intensity cross-calibration between in-loop and out-of-loop spectral flatness measurements. This provides the basis for future implementation and improvement on actual astronomical spectrographs. Our approach further reduces the dynamic range required for spectral flattening by pumping at a wavelength outside the desired calibration range, effectively nullifying the impact of high-frequency pump fluctuations on spectral stability. Finally, in addition to its applications in astronomy, similar spectral shaping setups with broad spectral coverage and high resolution have potential uses in telecommunications, 2D spectroscopy, material processing, and optical tweezers.

Optics EXPRESS

Funding. National Science Foundation (AST 2009982).

Acknowledgment. The authors acknowledge helpful discussions with Dahyeon Lee, Molly Kate Kreider and Andrew J Metcalf. The authors thank Matthew Heyrich for loaning the cavity-stabilized continuous wave laser.

Disclosures. The authors declare no conflicts of interest.

Data availability. Data underlying the results presented in this paper may be obtained from the authors upon reasonable request.

Supplemental document. See Supplement 1 for supporting content.

References

1. D. A. Braje, M. S. Kirchner, S. Osterman, *et al.*, "Astronomical spectrograph calibration with broad-spectrum frequency combs," Eur. Phys. J. D **48**(1), 57–66 (2008).
2. M. T. Murphy, T. Udem, R. Holzwarth, *et al.*, "High-precision wavelength calibration of astronomical spectrographs with laser frequency combs," Mon. Not. R. Astron. Soc. **380**(2), 839–847 (2007).
3. T. Herr and R. A. McCracken, "Astrocombs: recent advances," IEEE Photonics Technol. Lett. **31**(23), 1890–1893 (2019).
4. T. Steinmetz, T. Wilken, C. Araujo-Hauck, *et al.*, "Laser frequency combs for astronomical observations," Science **321**(5894), 1335–1337 (2008).
5. R. A. Probst, D. Milaković, B. Toledo-Padrón, *et al.*, "A crucial test for astronomical spectrograph calibration with frequency combs," Nat. Astron. **4**(6), 603–608 (2020).
6. G. G. Ycas, F. Quinlan, S. A. Diddams, *et al.*, "Demonstration of on-sky calibration of astronomical spectra using a 25 ghz near-ir laser frequency comb," Opt. Express **20**(6), 6631–6643 (2012).
7. E. Obrzud, M. Rainer, A. Harutyunyan, *et al.*, "Broadband near-infrared astronomical spectrometer calibration and on-sky validation with an electro-optic laser frequency comb," Opt. Express **26**(26), 34830–34841 (2018).
8. A. J. Metcalf, T. Anderson, C. F. Bender, *et al.*, "Stellar spectroscopy in the near-infrared with a laser frequency comb," Optica **6**(2), 233–239 (2019).
9. C. Lage, A. Bradshaw, and J. A. Tyson, "Measurements and simulations of the brighter-fatter effect in ccd sensors," J. Instrum. **12**(03), C03091 (2017).
10. A. Plazas, C. Shapiro, R. Smith, *et al.*, "Nonlinearity and pixel shifting effects in hxrg infrared detectors," J. Instrum. **12**(04), C04009 (2017).
11. J. P. Ninan, S. Mahadevan, G. Stefansson, *et al.*, "Impact of crosshatch patterns in h2rgs on high-precision radial velocity measurements: exploration of measurement and mitigation paths with the habitable-zone planet finder," J. Astron. Telesc. Instrum. Syst. **5**(04), 1 (2019).
12. P. Sekhar, M. Kate Kreider, C. Fredrick, *et al.*, "Tunable 30 ghz laser frequency comb for astronomical spectrograph characterization and calibration," Opt. Lett. **49**(21), 6257–6260 (2024).
13. R. A. Probst, T. Steinmetz, T. Wilken, *et al.*, "Spectral flattening of supercontinua with a spatial light modulator," in *Techniques and Instrumentation for Detection of Exoplanets VI*, vol. 8864 (SPIE, 2013), pp. 706–713.
14. M. Debus, P. Huke, D. Meyer, *et al.*, "Spectral envelope control for a flat frequency comb spectrum," J. Astron. Telesc. Instrum. Syst. **7**(02), 025005 (2021).
15. T. Serizawa, T. Kurokawa, Y. Tanaka, *et al.*, "Laser frequency comb system for the infrared doppler instrument on the subaru telescope," J. Astron. Telesc. Instrum. Syst. **10**(02), 025006 (2024).
16. A. M. Weiner, "Femtosecond pulse shaping using spatial light modulators," Rev. Sci. Instrum. **71**(5), 1929–1960 (2000).
17. T. A. Strasser and J. L. Wagener, "Wavelength-selective switches for roadm applications," IEEE J. Select. Topics Quantum Electron. **16**(5), 1150–1157 (2010).
18. K. Yamane, Z. Zhang, K. Oka, *et al.*, "Optical pulse compression to 3.4 fs in the monocycle region by feedback phase compensation," Opt. Lett. **28**(22), 2258–2260 (2003).
19. N. Ji, D. E. Milkie, and E. Betzig, "Adaptive optics via pupil segmentation for high-resolution imaging in biological tissues," Nat. Methods **7**(2), 141–147 (2010).
20. S. T. Cundiff and A. M. Weiner, "Optical arbitrary waveform generation," Nat. Photonics **4**(11), 760–766 (2010).
21. M. Ulman, D. Bailey, L. Acioli, *et al.*, "Femtosecond tunable nonlinear absorption spectroscopy in al 0.1 ga 0.9 as," Phys. Rev. B **47**(16), 10267–10278 (1993).
22. S.-H. Shim and M. T. Zanni, "How to turn your pump–probe instrument into a multidimensional spectrometer: 2d ir and vis spectroscopies via pulse shaping," Phys. Chem. Chem. Phys. **11**(5), 748–761 (2009).
23. D.-M. Spangenberg, A. Dudley, P. H. Neethling, *et al.*, "White light wavefront control with a spatial light modulator," Opt. Express **22**(11), 13870–13879 (2014).
24. Y. Yuan, L. Jiang, X. Li, *et al.*, "Laser photonic-reduction stamping for graphene-based micro-supercapacitors ultrafast fabrication," Nat. Commun. **11**(1), 6185 (2020).
25. Y. Zhao, L. Cao, H. Zhang, *et al.*, "Accurate calculation of computer-generated holograms using angular-spectrum layer-oriented method," Opt. Express **23**(20), 25440–25449 (2015).
26. H. Kim, W. Lee, H.-g. Lee, *et al.*, "In situ single-atom array synthesis using dynamic holographic optical tweezers," Nat. Commun. **7**(1), 13317 (2016).

Optics EXPRESS

27. N. Jovanovic, P. Gatkine, B. Shen, *et al.*, "Flattening laser frequency comb spectra with a high dynamic range, broadband spectral shaper on-a-chip," Opt. Express **30**(20), 36745–36760 (2022).
28. Z. Wang, Z. Fang, Y. Zhu, *et al.*, "An electro-optically tunable arrayed waveguide grating fabricated on thin film lithium niobate," APL Photonics **10**(1), 016105 (2025).
29. S. Mahadevan, L. Ramsey, C. Bender, *et al.*, "The habitable-zone planet finder: a stabilized fiber-fed nir spectrograph for the hobby-eberly telescope," Proc. SPIE **8446**, 84461S (2012).
30. S. Mahadevan, L. W. Ramsey, R. Terrien, *et al.*, "The habitable-zone planet finder: A status update on the development of a stabilized fiber-fed near-infrared spectrograph for the for the hobby-eberly telescope," Proc. SPIE **9147**, 91471G (2014).
31. P. Sekhar, C. Fredrick, D. R. Carlson, *et al.*, "20 ghz fiber-integrated femtosecond pulse and supercontinuum generation with a resonant electro-optic frequency comb," APL Photonics **8**(11), 116111 (2023).
32. D. R. Carlson, P. Hutchison, D. D. Hickstein, *et al.*, "Generating few-cycle pulses with integrated nonlinear photonics," Opt. Express **27**(26), 37374–37382 (2019).
33. Kowligy, Cingöz, and Roslund, "Integrated nonlinear photonic waveguide assembly for frequency comb stabilization," (U.S. Patent US11953804B1).
34. H. Zhen, H. Ye, F. Du, *et al.*, "Improving the spectral uniformity of calibration sources for astronomical spectrographs by spectrum shaping," in *AOPC 2024: Optical Spectroscopy and Applications*, vol. 13494 (SPIE, 2024), pp. 60–65.
35. R. A. Probst, "Laser frequency combs for astronomy," Ph.D. thesis, lmu (2015).